Proceedings of the International Conference of
Bioelectromagnetism, Electrical Bioimpedance, and Electrical Impedance Tomography
June 28 – July 1, 2022 / Kyung Hee University, Seoul, Korea

A Hybrid FE-EFG Method for 2D MIT Forward Problem Computation

Hassan Yazdanian[1], Maedeh Hadinia[2]

[1]Department of Biomedical Engineering, K. N. Toosi University of Technology, Tehran, Iran
[2]Department of Electrical Engineering, College of Electrical Engineering, Langarud Branch, Islamic Azad University, Langarud, Iran

Correspondence: Maedeh Hadinia, e-mail: maedeh.hadinia@iau.ac.ir

Abstract– Magnetic induction tomography (MIT) is a modality for imaging the electrical conductivity of biological tissues. This paper presents a hybrid finite element-element free Galerkin (FE-EFG) method for solving 2D MIT forward problem. The numerical implementation of the hybrid method is validated by an analytical problem. A 16-coil 2D MIT system is modeled and the hybrid method is employed to solve the forward problem using a head phantom. The results hold promise for alternatively employing of the hybrid FE-EFG method in situations with meshing task problem.

Keywords: Element-free Galerkin method, finite element method, forward problem, magnetic induction tomography.

1. Introduction

Magnetic induction tomography (MIT) is a relatively emerging modality that attempts to image the electrical conductivity distribution inside an object (Korjenevsky *et al* 2000). MIT features non-contact, non-invasive, non-radiative, and low-cost which make it attractive for biomedical applications. Recently, several studies have focused on imaging of intracranial haemorrhage using MIT (Zolgharni *et al* 2010, Xiao *et al* 2018, Chen *et al* 2021). The forward problem in MIT is a boundary value problem which has mostly been solved by mash-based methods such as finite element (FE) method (Xiao *et al* 2018) or finite difference method (Zolgharni *et al* 2010). Using these methods in problems with complex geometries, like the human head in which generation of a mesh is a challenging task, may be problematic (Von Ellenrieder *et al* 2005). Furthermore, in some applications like imaging of lung ventilation, the shape and size of regions of the object under study are subject to frequent deformations. It can cause some difficulties for mesh-based methods.

There is another group of numerical techniques called mesh-free methods. They approximate an unknown function based on a set of nodes distributed in the problem domain, and do not need usual connection between nodes to construct discrete equations. Numerous mesh-free methods have been presented to solve boundary value problems, such as the element-free Galerkin (EFG) method (Hadinia *et al* 2016) and wavelet Galerkin method (Yousefi *et al* 2013). To the best of the authors' knowledge, mesh-free methods have not been employed to solve the biomedical MIT forward problem. In this paper, for the first time, we use the EFG method for solving 2D MIT forward problem. This method has been employed to solve the EIT forward problem in several studies (Cutrupi *et al* 2007, Hadinia *et al* 2016). EFG has also been used for the computation of static and quasi-static electromagnetic fields (Xuan *et al* 2004).

The EFG basis functions do not satisfy the Kronecker delta criterion (Hadinia *et al* 2016). This property makes the imposition of essential boundary conditions difficult compared to for instance the FE method. It is possibly the main drawback of the EFG method. The most efficient and accurate method to address the difficulty is coupling with FE method (Dolbow and Belytschko 1998). In this paper, we apply this method which results in the hybrid FE-EFG method for solving the MIT forward problem.

2. Methods

2.1 MIT forward problem

The forward problem in MIT includes a classical eddy current problem. By considering the magneto-quasi-static approximation, the 2D MIT forward problem in the frequency domain is governed by (Yazdanian *et al* 2020):

$$\begin{cases} (1/\mu_0)\nabla^2 A_z = -J & \text{in} \quad \Omega_N \\ (1/\mu_0)\nabla^2 A_z - \mathrm{j}\omega\sigma A_z = 0 & \text{in} \quad \Omega_C \end{cases} \tag{1}$$

where A_z and J are the z-component of the magnetic vector potential (MVP) and the applied current density to an excitation coil, respectively, and $\mathrm{j}=\sqrt{-1}$. Domains Ω_N and Ω_C are the non-conducting and conducting (or eddy current) regions, respectively, and μ_0, σ, and ω are the free space magnetic permeability, electrical conductivity, and angular

frequency, respectively. The region Ω_C is the imaging region and Ω_N includes the MIT coils and air. Boundary conditions are required to obtain a unique solution for Equation (1). At the outer boundary of the problem, the far-field boundary condition is applied. In addition, at the interface of two different material, the continuity of normal component of magnetic flux density and tangential component of magnetic field intensity should be satisfied (Turner and Han 1987).

The output of the forward problem is the induced voltage in the sensing coils obtained by (Yazdanian *et al* 2020):

$$V = \mathrm{j}\omega \oint_C A_z \, \vec{a}_z \cdot \mathrm{d}\vec{\ell} \tag{2}$$

where C is a closed contour bounding the internal area of the sensing coil. The induced voltage is a complex value. In the low-conductivity applications of MIT, including biomedical applications, the real-part of V is proportional to the conductivity distribution in the imaging region (Yazdanian *et al* 2020). Equation (2) shows that the real-part of V is proportional to the imaginary-part of A_z. Therefore, we consider the real-part of V and imaginary-part of A_z in Section 3.

2.2 Numerical implementation

In the proposed hybrid FE-EFG method, regions Ω_N and Ω_C are formulated by FE and EFG methods and donated by Ω^{FE} and Ω^{EFG}, respectively. Then, the computational domain will be $\Omega = \Omega^{\mathrm{FE}} \cup \Omega^{\mathrm{EFG}}$. Formulating Ω_N by the FE method resolves the problem of imposing of essential boundary conditions for EFG method (Hadinia *et al* 2016) while formulating Ω_C by the EFG method handles the region with meshing task problem and/or moving objects.

Discretization with FE and EFG methods

The region Ω^{FE} is discretised by M triangular elements and includes N^{FE} nodes. The MVP A^{FE} at each point $\mathbf{x}$ inside Ω^{FE} is given by a linear interpolation of nodal value $\hat{A}_i^{FE}$ (Hadinia *et al* 2016):

$$A^{\mathrm{FE}}(\mathbf{x}) = \sum_{i=1}^{N^{\mathrm{FE}}} \phi_i^{\mathrm{FE}}(\mathbf{x}) \hat{A}_i^{\mathrm{FE}} \quad \forall \, \mathbf{x} \in \Omega^{\mathrm{FE}} \tag{3}$$

where $\phi_i^{\mathrm{FE}}(\mathbf{x})$ $(i = 1{:}\, N^{\mathrm{FE}})$ are linear nodal shape functions.

The region Ω^{EFG} is discretised by N^{EFG} nodes. The shape functions in the EFG method are constructed by moving least square approximation. Then, the MVP A^{EFG} at each point $\mathbf{x}$ inside Ω^{EFG} is approximated by (Hadinia *et al* 2016):

$$A^{\mathrm{EFG}}(\mathbf{x}) = \sum_{i=1}^{N^{\mathrm{EFG}}} \phi_i^{\mathrm{EFG}}(\mathbf{x}) \hat{A}_i^{\mathrm{EFG}} \quad \forall \, \mathbf{x} \in \Omega^{\mathrm{EFG}} \tag{4}$$

where the nodal parameter $\hat{A}_i^{\mathrm{EFG}}$ is the approximation to $A^{\mathrm{EFG}}(\mathbf{x})$ at the node $\mathbf{x}_i$ and $\phi_i^{\mathrm{EFG}}(\mathbf{x})$ is EFG shape function.

FE-EFG method

By discretization of Equation (1), a system of equations will be obtained for each region as follows:

$$\boldsymbol{\mathcal{K}}^{\mathrm{FE}} \; \boldsymbol{\mathcal{A}}^{\mathrm{FE}} \; = \boldsymbol{\mathcal{F}} \quad \text{in } \Omega^{\mathrm{FE}} \tag{5}$$

$$\boldsymbol{\mathcal{K}}^{\mathrm{EFG}} \, \widehat{\boldsymbol{\mathcal{A}}}^{\mathrm{EFG}} = \mathbf{0} \quad \text{in } \Omega^{\mathrm{EFG}} \tag{6}$$

where $\boldsymbol{\mathcal{K}}^{\mathrm{FE}}$ and $\boldsymbol{\mathcal{K}}^{\mathrm{EFG}}$ were defined in (Wang *et al* 2007) and (Hadinia *et al* 2016), respectively, $\boldsymbol{\mathcal{A}}^{\mathrm{FE}}$ and $\widehat{\boldsymbol{\mathcal{A}}}^{\mathrm{EFG}}$ contain node potentials in Ω^{FE} and the nodal parameters in Ω^{EFG}, respectively, and $\boldsymbol{\mathcal{F}}$ contain current density of an exaction coil. To couple FE and EFG methods, the following continuity conditions have to be enforced on the interface boundary Γ^{int} between two regions Ω^{FE} and Ω^{EFG} (Hadinia *et al* 2016):

$$A_z^{\mathrm{FE}}(\mathbf{x}) = A_z^{\mathrm{EFG}}(\mathbf{x}) \quad \mathbf{x} \in \Gamma^{int} \tag{7}$$

$$\frac{1}{\mu_{\mathrm{FE}}} \nabla A_z^{\mathrm{FE}}(\mathbf{x}) \cdot \vec{\mathrm{n}}\Big|_{\Gamma^{int}} = \frac{1}{\mu_{\mathrm{EFG}}} \nabla A_z^{\mathrm{EFG}}(\mathbf{x}) \cdot \vec{\mathrm{n}}\Big|_{\Gamma^{int}} \tag{8}$$

where $\vec{\mathrm{n}} = \vec{\mathrm{n}}^{FE} = -\vec{\mathrm{n}}^{EFG}$ is outward unit vector which is normal to the Γ^{int}, and μ_{FE} and μ_{EFG} are the permeability in FE and EFG regions, respectively. To couple (5) and (6) and impose (7) and (8) as well, the Lagrange multiplier method is employed. Therefore, one can find the following system of equations (Hadinia *et al* 2016):

$$\begin{bmatrix} \boldsymbol{\mathcal{K}}^{\mathrm{FE}} & \mathbf{0} & \boldsymbol{\mathcal{H}}^{\mathrm{FE}} \\ \mathbf{0} & \boldsymbol{\mathcal{K}}^{\mathrm{EFG}} & \boldsymbol{\mathcal{H}}^{\mathrm{EFG}} \\ (\boldsymbol{\mathcal{H}}^{\mathrm{FE}})^T & (\boldsymbol{\mathcal{H}}^{\mathrm{EFG}})^T & \mathbf{0} \end{bmatrix} \begin{bmatrix} \boldsymbol{\mathcal{A}}^{\mathrm{FE}} \\ \widehat{\boldsymbol{\mathcal{A}}}^{\mathrm{EFG}} \\ \boldsymbol{\eta} \end{bmatrix} = \begin{bmatrix} \boldsymbol{\mathcal{F}} \\ \mathbf{0} \\ \mathbf{0} \end{bmatrix} \tag{9}$$

where $\boldsymbol{\mathcal{H}}^{\mathrm{FE}}$ and $\boldsymbol{\mathcal{H}}^{\mathrm{EFG}}$ are explained in (Hadinia *et al* 2016).

3. Numerical experiments

3.1 Benchmark test

In order to validate the hybrid FE-EFG numerical techniques, a benchmark test was first attempted. The benchmark test was designed by inspiration of the one presented in (Peyton *et al* 1996). The problem region consists of seven concentric circle as shown in Figure 1. One may picture the region as the inside of an infinitely long cylinder whose outside extends to infinity. The conductivity and radii for each layer are similar to values given in (Dekdouk *et al* 2008). They are chosen to simulate a slice of head model. The excitation field is generated by a current density distribution of $J = J_0 \sin\varphi$ (A/m) at $r_7 = 100$ mm. The general solution for the test problem in the polar coordinate will be as follows:

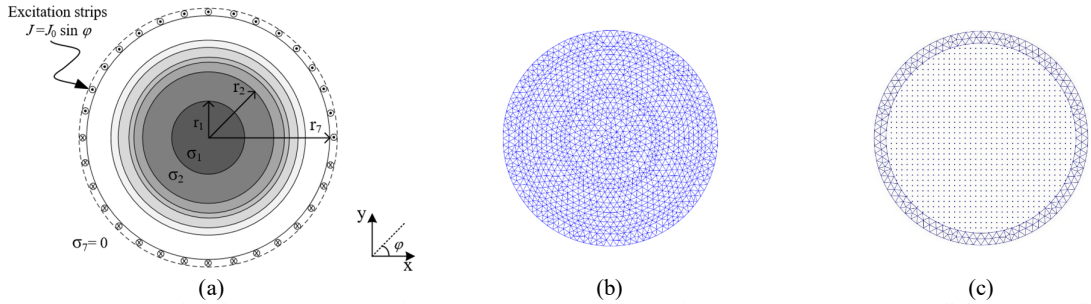

Figure 1. (a) 2D benchmark test assembly containing six conductive layers (σ_1 to σ_6) in a parallel magnetic field. The condictivity and radius of each laye are similar to values given in (Dekdouk *et al* 2008). Domain discretization for (b) the FE method and (c) the hybrid FE-EFG method.

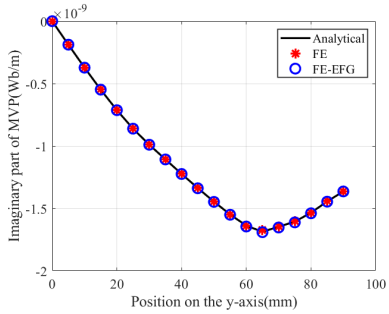

Figure 2. Imaginary part of MVPs calculated by (black line) analytical solution, (red stars) FE method, and (blue circles) FE-EFG method for points located on *y*-axis, from (0, 0) to (0, 90) mm (step by 5 mm).

$$A_z(r,\varphi) = \sum_{n=1}^{\infty} [a_n I_n(\alpha_k r) + b_n K_n(\alpha_k r)] \sin(n\varphi) \tag{10}$$

where I_n and K_n are modified Bessel functions of the first and second kinds, respectively, a_n and b_n are constant coefficients to be determined from the boundary conditions, and $\alpha_k = \sqrt{\omega \sigma_k \mu_0}$. Since the excitation filed is generated by $\sin \varphi$, (10) exists only for $n = 1$.

The test problem was then solved numerically by FE and FE-EFG methods. In the analytical problem, the excitation filed is unrealistically generated by surface current densities. Therefore, instead of using excitation strips as shown in Figure 1(a), we calculated MVPs by the analytical solution at $r = 90$ mm and then imposed them to numerical methods as the Dirichlet boundary conditions. FE mesh, as shown in Figure 1(b), has 1360 nodes and 2618 elements. In the hybrid method, as shown in Figure 2(c), the EFG domain has a uniform distribution of 1136 nodes and FE domain has 265 nodes and 366 elements. There are 76 common nodes on the interface boundary Γ^{int}. Figure 2 compares MVPs obtained from numerical solutions to those of obtained by the analytical solution. We calculated the percentage of the relative error for FE and FE-EFG methods for points located on *y*-axis, from (0, 0) to (0, 90) mm (step by 5 mm). The relative error for the imaginary part of MVPs obtained by FE and FE-EFG method was 0.26% and 0.24%, respectively. The runtime for FE and FE-EFG method was 0.17 s and 0.29 s, respectively.

3.2 Head model

Figure 3(a) shows the cross-sectional view of the 2D MIT system, which has 16 air-core coils used for both excitation and sensing. The imaging region has a radius of R_1=110 mm, which models by the EFG method in the hybrid numerical method. The homogeneous Dirichlet boundary condition was imposed at a radius of 250 mm. The space outside of the imaging region, including coils, is modelled by the FE method in the hybrid method. Sequential activation of coils using a sinusoidal alternating current of 10 A amplitude and frequency of 10 MHz excites the imaging region. Only independent measurements are gathered. They are labelled from 1 to 120.

As shown in Figure 3(b), an axial cross-section of a realistic head model (available in simnibs.org) is embedded in the MIT setup. Similar 2D model has been used in (Xiao *et al* 2018). The head model contained five tissue types, as shown in Figure 3(c). The conductivity of brain tissues were chosen similar to values given in (Dekdouk *et al* 2008).We solved the forward problem using both FE and hybrid FE-EFG methods and calculated the induced voltages using Equation (2). In addition, we have used an extremely fine mesh to solve the forward problem by the FE method as a ground truth. The FE mesh in the pure FE method has 5997 nodes and 11932 elements. In the FE-EFG method, the discretized FE domain includes 2263 nodes and 4382 elements. The discretized EFG domain has a uniform distribution and includes 3804 nodes. The ground truth solution is obtained with a FE with a mesh including 23447 nodes and 46576 elements. Figure 4(a) shows the real part of induced voltages for all independent measurements calculated by FE method, FE-EFG method, and ground truth. Figure 4(b) depicts the absolute error (AE) of induced voltages for each numerical method compared to the ground truth. We also calculated the relative error for each numerical method in comparison with the ground truth. The percentage of relative error of the FE and FE-EFG methods was 1.83% and 1.49%, respectively. The run-time for the FE and FE-EFG methods was 4.80 s and 3.67 s, respectively.

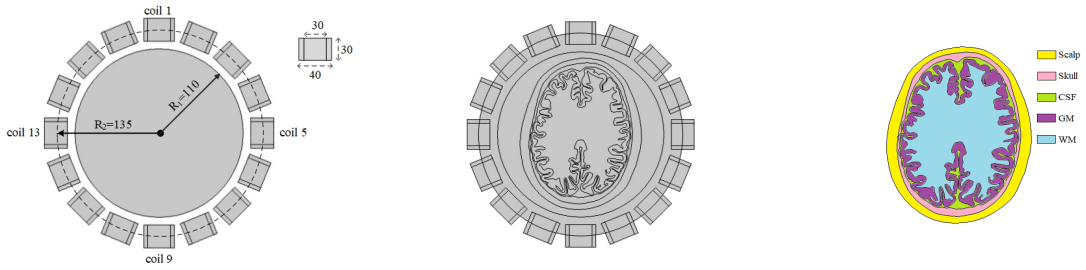

(a) (b) (c)

Figure 3. (a) 2D MIT system setup. Dimensions are in mm. (b) Head model inside MIT setup. (c) Different part of head model.

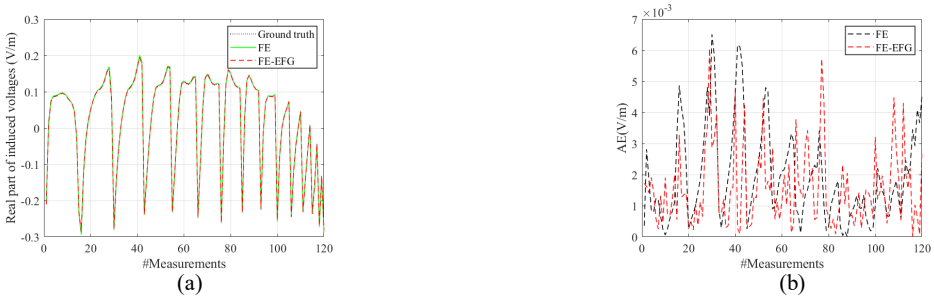

(a) (b)

Figure 4. (a) Real part of induced voltages calculated by the FE method, FE-EFG method, and ground truth. (b) Absolute error of the FE and FE-EFG methods compared to the ground truth.

4. Conclusions

In this paper, for the first time, a hybrid FE-EFG numerical method was developed to solve the 2D MIT forward problem. In the proposed numerical method, the EFG method was employed to solve the problem in the imaging region, and the FE method was used to solve the problem in coil and air around imaging region. In this way, we benefited from the advantages of both methods. Comparison of FE and FE-EFG methods through the numerical experiment revealed the superiority of the hybrid method. Results of this paper manifested that the hybrid FE-EFG method holds promise for solving MIT forward problem in domains with mesh difficulty task.

References

Chen Y, Tan C and Dong F 2021 Combined planar magnetic induction tomography for local detection of intracranial hemorrhage *IEEE Trans. Instrum. Meas.* **70**, 1-11

Cutrupi V, Ferraioli F, Formisano A and Martone R 2007 An approach to the electrical resistance tomography based on meshless methods *IEEE Trans. Magn.* **43**, 1717 - 1720

Dekdouk B, Pham M H, Armitage D W, Ktistis C, Zolgharni M and Peyton A J 2008 A feasibility study on the delectability of edema using magnetic induction tomography using an analytical model *IFMBE Proceedings*

Dolbow J and Belytschko T 1998 An introduction to programming the meshless element free Galerkin method *Arch. Comput. Methods Eng.* **5**, 207–241

Von Ellenrieder N, Muravchik C H and Nehorai A 2005 A meshless method for solving the EEG forward problem *IEEE Trans. Biomed. Eng.* **52**, 249-57

Hadinia M, Jafari R and Soleimani M 2016 EIT image reconstruction based on a hybrid FE-EFG forward method and the complete-electrode model *Physiol. Meas.* **37**, 863–78

Korjenevsky A, Cherepenin V and Sapetsky S 2000 Magnetic induction tomography: Experimental realization *Physiol. Meas.* **21**, 89-94

Peyton A J, Yu Z Z, Lyon G, Al-Zeibak S, Ferreira J, Velez J, Linhares F, Borges A R, Xiong H L, Saunders N H and Beck M S 1996 An overview of electromagnetic inductance tomography: Description of three different systems *Meas. Sci. Technol.* **7**, 261–71

Turner L and Han H C 1987 The Calculation of Transient Eddy-Current Fields Using Null-Field Integral Techniques *IEEE Trans. Magn.*

Wang C, Liu R, Fu F, You F, Shi X and Dong X 2007 Image reconstruction for magnetic induction tomography and preliminary simulations on a simple head model *IEMBS Proceedings* pp 4406–9

Xiao Z, Tan C and Dong F 2018 Multi-frequency difference method for intracranial hemorrhage detection by magnetic induction tomography *Physiol. Meas.* **39**, 055006

Xuan L, Zeng Z, Shanker B and Udpa L 2004 Element-free Galerkin method for static and quasi-static electromagnetic field computation *IEEE Trans. Magn.* **40**, 12 - 20

Yazdanian H, Jafari R and Moghaddam H 2020 Solution of 2D MIT forward problem by considering skin and proximity effects in coils *IEEE Trans. Comput. Imaging* **7**, 22 - 31

Yousefi M R, Jafari R and Moghaddam H A 2013 A combined wavelet-based mesh-free method for solving the forward problem in electrical impedance tomography *IEEE Trans. Instrum. Meas.* **62**, 2629 - 2638

Zolgharni M, Griffiths H and Ledger P D 2010 Frequency-difference MIT imaging of cerebral haemorrhage with a hemispherical coil array: Numerical modelling *Physiol. Meas.* **31**, S111